Materials Science & Engineering A 743 (2019) 98–105

Contents lists available at ScienceDirect

Materials Science & Engineering A

journal homepage: www.elsevier.com/locate/msea

Effects of nanosized TiC_p on the microstructure evolution and tensile properties of an Al-Mg-Si alloy during cold rolling

Run Geng[a,b], Feng Qiu[a,b], Qing-Long Zhao[a,b,*], Yu-Yang Gao[b], Qi-Chuan Jiang[a,b,*]

[a] State Key Laboratory of Automotive Simulation and Control, Jilin University, PR China
[b] Key Laboratory of Automobile Materials, Ministry of Education and School of Materials Science and Engineering, Jilin University, No. 5988 Renmin Street, Changchun 130025, PR China

ARTICLE INFO

Keywords:
Cold rolling
Nanoparticles
Al matrix composites
Recrystallization

ABSTRACT

The effects of a small addition of nanosized TiC particles (TiC_p) on the microstructure evolution of the Al-Mg-Si (6061) alloy throughout the entire fabrication process including casting, cold rolling and heat treatments were investigated. TiC_p impeded the recrystallization and grain growth, refined the grain structure, and evidently increased the tensile strength without obvious decrease on ductility. The ultimate tensile strength and yield strength of the 1.0 wt% TiC_p/6061 composite were 330 MPa and 275 MPa in T6 state and 438 MPa and 426 MPa in the as-rolled state, an increase of 42 MPa and 38 MPa, 41 MPa and 52 MPa, respectively, compared to the matrix 6061 alloy. The strength increase is attributed to strengthening effect of TiC_p, dislocation accumulation and precipitate strengthening.

1. Introduction

Al-Mg-Si plates/sheets are widely used in industrial fields due to their relatively high strength, considerable corrosion resistance and fatigue properties [1,2]. Among them, AA6061 aluminium alloy is a heat-treatable alloy that can obtain high strength through T6 or T4 treatment [3]. This alloy shows a relatively low strength but a high ductility in solution-treated conditions. The strength of this alloy can be enhanced by performing age hardening, and the ductility will decrease significantly [4]. Since this alloy is mainly used in age hardening conditions to utilize a higher strength to weight ratio, it is crucial to enhance the strength without sacrificing the ductility after the T6 process with the purpose of expanding the application of the 6061 Al sheets, especially where large deformation and high strength are required [5–7]. The reinforcement particles are known to enhance mechanical properties of Al alloys. Among the reinforcement particles, TiC is proved to be an excellent ceramic reinforcement, in terms of its suitable properties such as high hardness, good wear resistance and abrasion resistance [8–10].

The literature has clearly proved that the strengthening effects of nanoparticles are more obvious than micron-sized particles [11–13]. A low content of nanoparticles can increase the tensile strength of the matrix significantly through the Orowan mechanism, resulting from the larger quantity compared with the micron-sized particles. Moreover, the composites reinforced with nanoparticles possess higher ductility in comparison with the same materials reinforced with micron-sized particles. [14]. However, the effects of nano-sized reinforcements on the mechanical properties, as well as the strengthening mechanisms working in Al-Mg-Si sheets, is still need further research. In our previous work, we introduced the nanosized TiC particles (TiC_p) into the cast Al alloy using the nanosized TiC_p-Al master alloy, leading to a good distribution of nanoparticles and a significant improvement on tensile strength and ductility [15]. Compared with the micro-sized particles, the nanoparticles could improve the tensile strength without sacrificing the ductility [16].

The nanoparticles could act as the heterogeneous nucleation sites of α-Al and refine the grain structure in cast Al alloys [15,17]. The Orowan strengthening caused by the nanoparticles contributes to the improvements in tensile strength, while a high content of the nanoparticles tends to agglomerate, resulting in a reduction in the strength and elongation of nanocomposites [18]. Additionally, many researchers have studied the hot-extruded Al matrix composites [7,19,20]. The extruded nanocomposites usually contain a high fraction of the nanoparticles and exhibit a high tensile strength but a low ductility at both room temperature and elevated temperatures [5]. The nanoparticles could act as the barriers to dislocation movement during the deformation process and retard the recrystallization and grain growth, increasing the thermal stability of the refined grain structure at elevated temperatures [21,22].

However, research investigating the rolled Al matrix

* Corresponding authors.`
E-mail addresses: zhaoqinglong@jlu.edu.cn (Q.-L. Zhao), jqc@jlu.edu.cn (Q.-C. Jiang).

https://doi.org/10.1016/j.msea.2018.11.078
Received 19 September 2018; Received in revised form 15 November 2018; Accepted 16 November 2018
Available online 17 November 2018
0921-5093/

nanocomposites is limited. Dan et al. [23] studied the microstructure of cold rolled Al composites reinforced with 5 wt% nanosized TiB_{2p}. Most of the TiB_{2p} agglomerated around the Al grain boundaries and formed the particle clusters, while the rest were relatively uniformly dispersed inside the Al grains. High-density dislocations and high-angle grain boundaries were formed around the particle-clusters, and small dynamic recrystallized grains were found around particle-clusters resulting by the high local deformation strain. The literature mostly focused on the effects of the nanoparticles either on the as-cast grain structure or on the deformation structure [24–26]. Few researchers investigated the effects of the nanoparticles on the microstructure evolution during the entire fabrication process including casting, deformation (cold rolling) and heat treatments.

In this paper, the effect of TiC_p on the microstructure evolution of Al (6061) matrix composites during casting, rolling and the T6 heat treatment was studied. It was found that the nanosized TiC_p could retard the grain growth and increase the tensile strength without decreasing the ductility. The contributions of different strengthening mechanisms were also discussed. In comparison with the previous studies, the present work aims to investigate the effects of nanosized TiC_p throughout the entire fabrication process and provide a relatively easy way to improve the tensile properties of the Al plates/sheets.

2. Experimental

In the present work, the fabrication process is shown in Fig. 1. The 30 wt% nanosized TiC_p-6061 master alloy was produced by the self-propagation high-temperature synthesis (SHS) reaction of the metal powders of 6061 Al alloy, Ti and carbon nanotubes, which corresponded to stoichiometric TiC [27]. The mean size and morphology of TiC_p is shown in Fig. 2. The TiC_p were extracted from the master alloy using 18 vol% HCl aqueous solution. The morphology of the TiC_p was examined by FESEM (JSM-6700F, Japan). The nanosized TiC_p/6061 composites with mass fractions of 0.5% and 1.0% were produced by introducing the 30 wt% nanosized TiC_p-6061 master alloy into the molten 6061 Al, followed by the mechanical stirring for 2 min and ultrasonic vibration for 5 min (Fig. 1(a)). Finally, after the molten 6061 Al was cooled down to 1073 K, it was cast into a preheated steel mold ($200 \times 190 \times 20\ mm^3$). The temperature of the preheated mold was 200 °C. For comparison, the 6061 Al alloy was also prepared by the same casting procedure. The nominal composition of the 6061 Al alloy is 0.87 Mg, 0.55 Si, 0.59 Fe, 0.36 Cu, 0.15 Mn, 0.17 Cr, 0.23 Zn, 0.16 Ti and balanced Al (in wt%). The samples for cold rolling with the dimensions of $\sim 6 \times 20 \times 50\ mm^3$ were cut from the bottom of the castings. Homogenization treatment was performed at 570 °C for 7 h and cooled down by air (Fig. 1(b)). Then, the cold rolling (CR) was carried out with 70% thickness reduction by 5 rolling passes (1 mm for each pass of the first four passes, and 0.2 mm for the last pass) at room temperature (Fig. 1(c)). After the CR process, the T6 heat treatment (solution at 525 °C for 1 h [5], then quenching in the water and ageing at 180 °C for 5 h) was carried out and the CR-T6 samples were obtained. By considering the followed deformation process of the sheets in industrial applications, the CR-T6 samples underwent a secondary rolling (SR) process with a 50% thickness reduction at room temperature for the further investigations (Fig. 1(d)).

The microstructures at the mid-thickness of the rolling direction (RD)-normal direction (ND) section were observed, using a scanning electron microscope (SEM, Tescan vega3 XM) equipped with electron backscatter diffraction (EBSD, Oxford). The step size for EBSD scanning was 1 μm. EBSD data and grain size statistics were carried out using the *HKL* Channel 5 software, and the critical angles of 2° and 15° were adopted in the boundary detection. Transmission electron microscopy (TEM, JEM-2100F) was performed to observe the microstructures. TEM thin foils were prepared at −20 °C using twin-jet electropolishing with a solution of 90 vol% ethanol and 10 vol% perchloric acid at 20 V. The bone-shaped tensile specimens were prepared with a gauge cross section of $4.0 \times 1.8\ mm^2$ and a gauge length of 10 mm. A tensile test was performed in the rolling direction by a servo-hydraulic material testing system (MTS, MTS810) at room temperature using a strain rate of $3.0 \times 10^{-4}\ s^{-1}$ and at least three samples were tested for each state.

3. Results and discussion

3.1. The microstructure evolution

Fig. 3(a)–c) show that the as-cast grain structure was refined by the introduction of the nanosized TiC_p. The average grain size of the as-cast 6061 Al alloy was 108 μm, while it was refined to 57 μm and 40.1 μm by adding 0.5 and 1.0 wt% nanosized TiC_p, respectively. The grain size of the CR samples also decreased with the increasing content (from 0.5 to

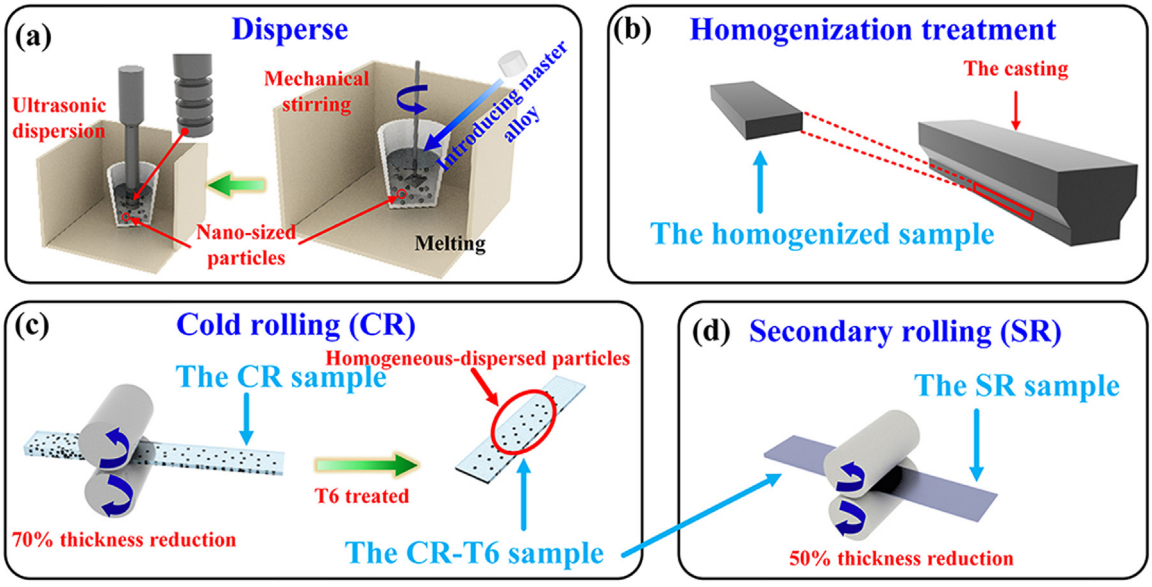

Fig. 1. Schematic diagram of the fabrication process, (a) the nanosized TiC_p-6061 master alloy was added into the molten metal with the mechanical stirring and ultrasonic vibration, (b) the homogenization treatment of the as-cast samples, (c) the samples after the first cold rolling process and T6 treatment, (d) the sample after the secondary rolling process.

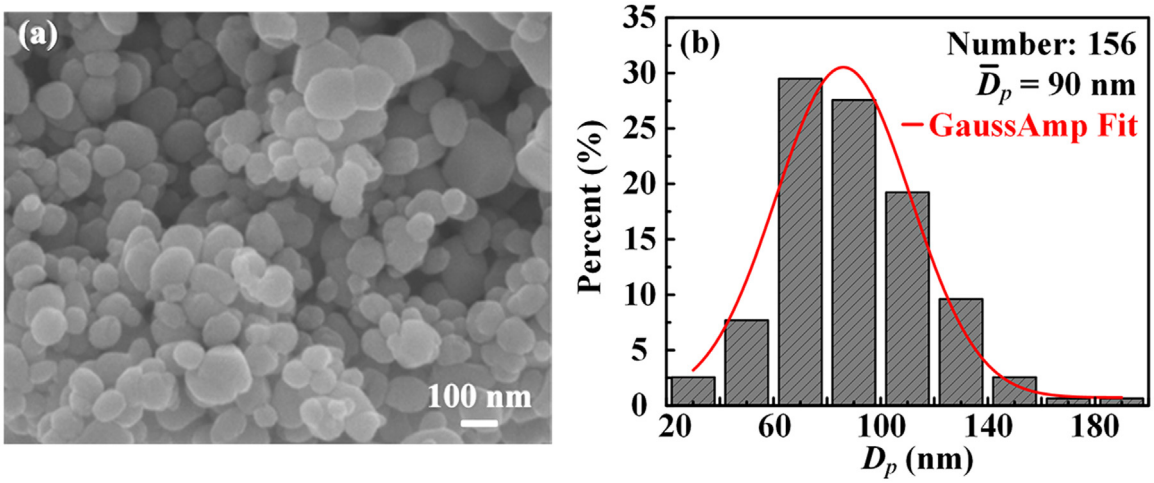

Fig. 2. FESEM image of the TiC_p extracted from the master alloy (a); the size distribution diagrams of the TiC_p (b).

1.0 wt%) of the nanosized TiC_p during the cold rolling processing as shown in Fig. 3(d)-(e). The grain size in the matrix 6061 Al alloy was ~39 μm in width after the CR process, and it was refined to ~25 μm and ~13 μm in width by introducing 0.5 and 1.0 wt% nanosized TiC_p, respectively. Recrystallization occurred in the deformed samples during the solution treatment. Fig. 4 shows the EBSD images of the CR-T6 samples including the 6061 Al alloy, 0.5 wt% nanosized TiC_p/6061 composite (0.5–6061 Al) and 1.0 wt% nanosized TiC_p/6061 composite (1.0–6061 Al) after T6 treatment. The addition of the nano-sized TiC_p refined the recrystallized grains. The small-sized grains existed around the coarse grains and the small-sized grains tended to be more prevalent and smaller in size as the content of the nanosized TiC_p increased, as shown in Fig. 4(a)–(c).

The grain size distributions of these T6 treated materials are shown in Fig. 4(g)-(i). The grains of the matrix 6061 Al alloy were coarse with an average size of 41 ± 4 μm, while the grains of the composites decreased with the increasing content of the nanosized TiC_p. The average sizes of the α-Al grains were ~ 15 ± 2 μm and 13 ± 2 μm in the 0.5–6061 Al and 1.0–6061 Al, respectively. In addition, the matrix 6061 Al alloy showed a wide range of grain size distribution and possessed 10% grains with a size over 100 μm. The composites have a narrower grain size distribution, in comparison with the matrix 6061 Al alloy, e.g., ~ 80% grains in the 0.5–6061 Al and 1.0–6061 Al with a size no more than 25 μm. Moreover, 1.0–6061 Al possessed the highest percentage (25%) of smallest grains (< 25 μm). The white lines in Fig. 4(a)-(c) represent the sub-grain boundaries. Few sub-grain boundaries were observed in the EBSD image of the 6061 Al alloy (Fig. 3(a)). However, more sub-grain boundaries were found in the

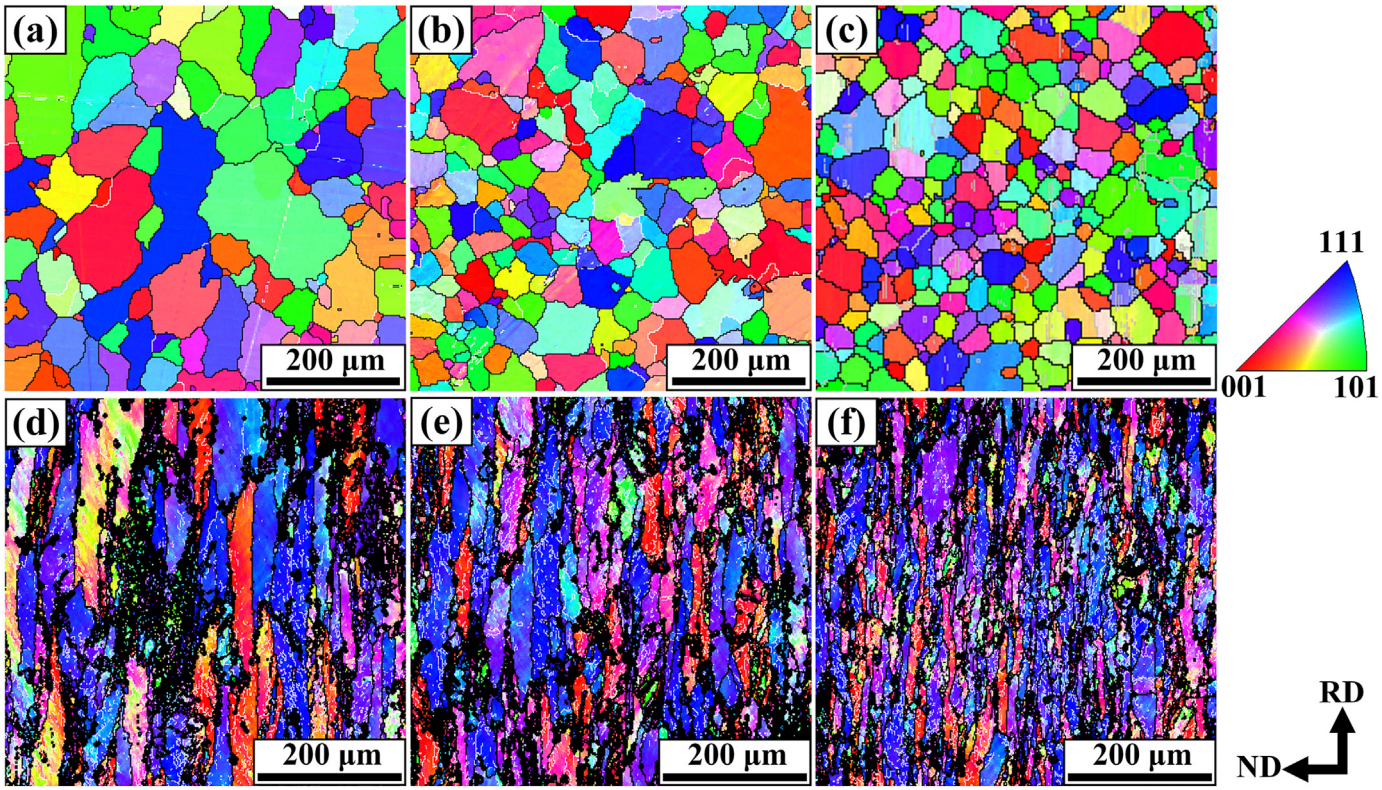

Fig. 3. EBSD images of the as-cast (a) 6061 Al alloy, (b) 0.5 wt% TiC_p/6061 composite, (c) 1.0 wt% TiC_p/6061 composite and the cold rolled without annealing (d) 6061 Al alloy, (e) 0.5 wt% TiC_p/6061 composite, (f) 1.0 wt% TiC_p/6061 composite.

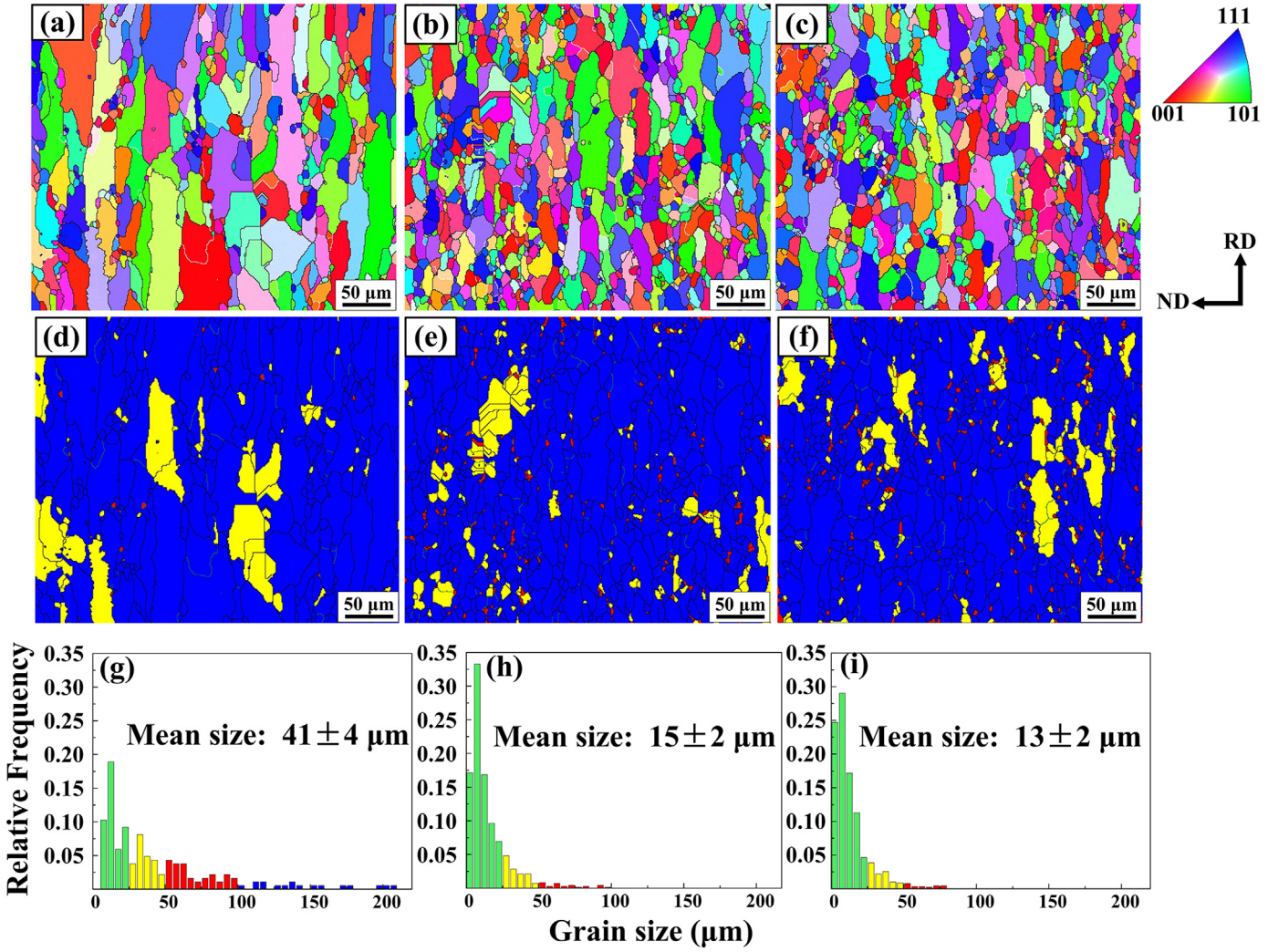

Fig. 4. EBSD images of (a) and (d) the 6061 Al alloy, (b) and (e) the 0.5 wt% TiC_p/6061 composite, (c) and (f) the 1.0 wt% TiC_p/6061 composite after T6 treatment; (g)–(i) the grain size distribution of these samples.

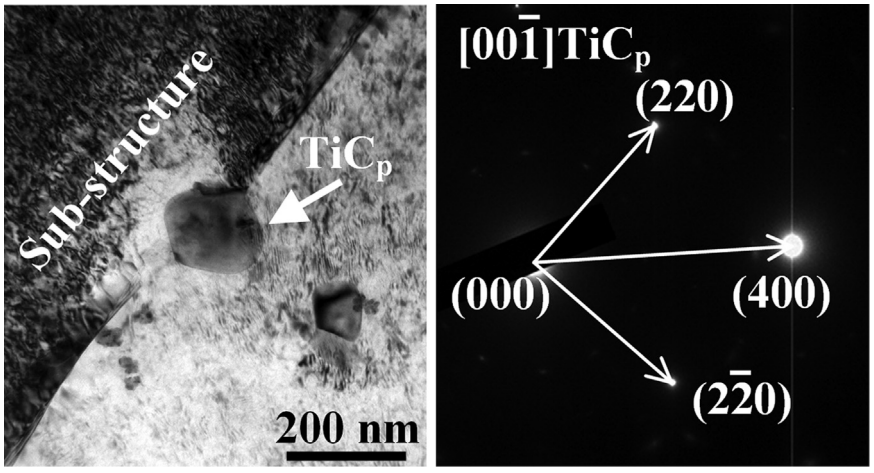

Fig. 5. Nanosized TiC_p pinned the sub-structures at grain boundary after the T6 treatment.

composites. In Fig. 4(d)-(f), the blue zones represent the fully recrystallized grains, the yellow zones represent the recovered grains and the red zones represent the deformation regions. This suggests that the matrix 6061 Al alloy after T6 treated was almost fully recrystallized, while in the composites, some deformation regions were retained. The deformation regions in the 1.0–6061 Al distributed more homogeneously and were larger in number and smaller in size, in comparison with the 0.5–6061 Al. The refined microstructure was attributed to two causes: I). the nanosized TiC_p could refine the as-cast grain structure which contributes to refined grains after deformation, thus providing

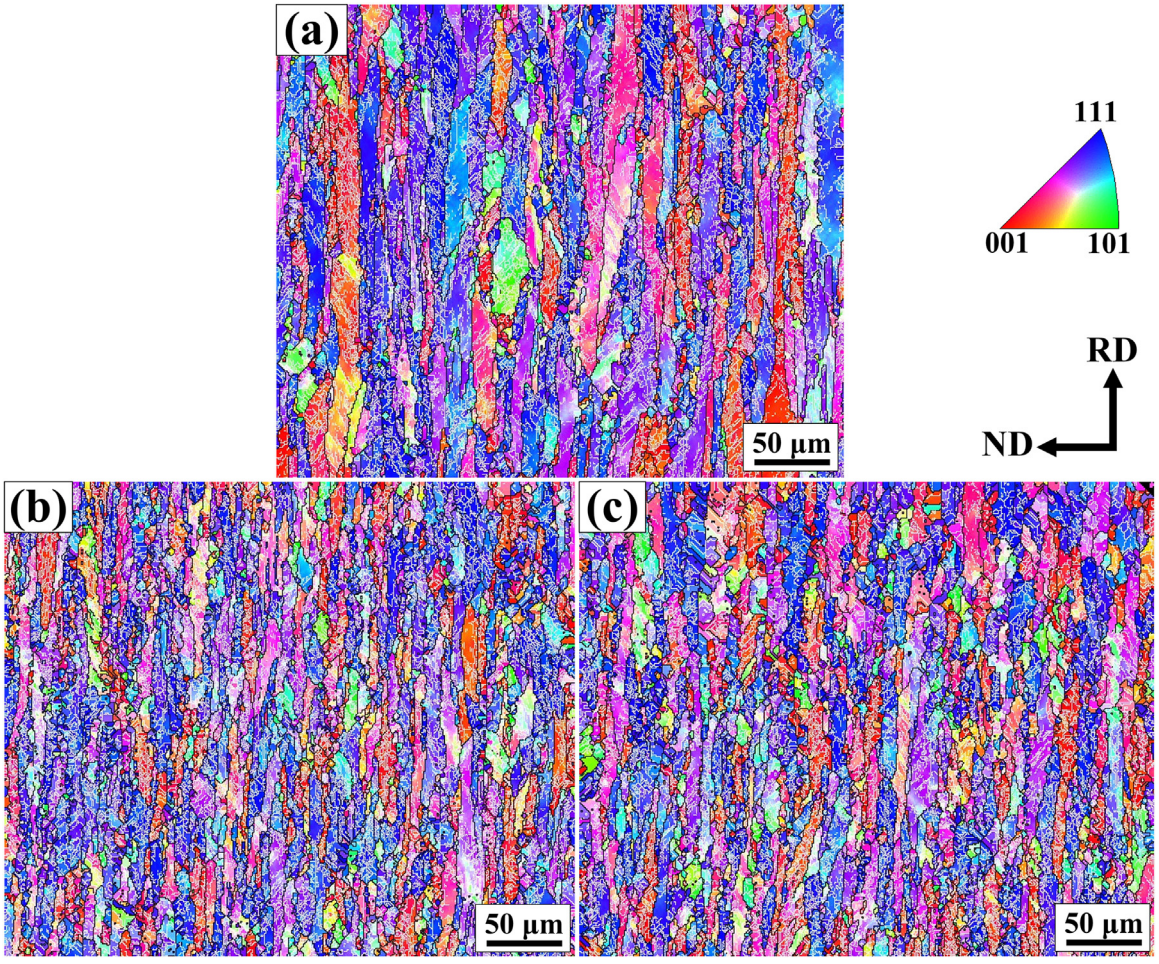

Fig. 6. EBSD orientation imaging maps of the (a) 6061 Al alloy, (b) 0.5 wt% TiC_p/6061composite and (c)1.0 wt% TiC_p/6061 composite in SR state. The white line represents the sub-grain boundaries.

more nuclei for the recrystallized grains according to the recrystallized nuclei could form at grain boundaries [28], and II). the nanosized TiC_p can induce the Zener pinning effect on the grain boundaries as shown in Fig. 5. The small deformation regions and the refined recrystallized grains are retained after the recrystallization by the retardation of the nanosized TiC_p. Thus, the introduction of the nanosized TiC_p could refine the recrystallized grains.

Fig. 6 shows the EBSD images of the SR samples. As indicated in Fig. 6(a)-(c), the density of the sub-grain boundaries in the composites is higher than that in the matrix 6061 Al alloy. The grain size decreased with the increasing content of the nanosized TiC_p. Fig. 7(a) shows the dislocation movement without the influence of the nanosized TiC_p. However, when the nanosized TiC_p were introduced, the dislocations were retarded by the nanosized particles as indicated in Fig. 7(b). A high-density dislocation is also found around the nanosized TiC_p (Fig. 7(c)). These dislocations interact with each other when two adjacent particles are close (Fig. 7(d)). Thus, we can conclude that the impediment of the nanosized TiC_p on the dislocation movement leads to the formation of the sub-structures.

3.2. Tensile properties

Fig. 8 shows the engineering stress-strain curves of the matrix 6061 Al alloy for different fabrication processes at room temperature. The ultimate strength (UTS) and yield strength (YS) improved obviously with the increasing content of the nanosized TiC_p. The UTS and YS are 330 ± 2 MPa and 275 ± 3 MPa in 1.0–6061 Al after T6 treatment, respectively. They are ~ 15% and 16% higher than those of the matrix 6061 Al alloy, as listed in Table 1. The tensile test results of the SR samples also demonstrate the evident reinforcing effects of nanosized TiC_p. The UTS and YS of 1.0–6061 Al can reach up to 438 ± 2 MPa and 426 ± 4 MPa, respectively, ~10% and 14% higher than those of the 6061 SR samples.

The strengthening effects of the nanosized TiC_p can be attributed to many sources, including the grain refinement, Orowan strengthening and dislocation strengthening. The refined grains in these composites show a significant effect on deformation procedure. On the one hand, the grain boundaries play as a barrier to impede the further movement of the dislocation, resulting in the improvement of the tensile strength in these composites. On the other hand, the small grain size is beneficial for the formability providing better ductility. According to Figs. 4, 10.0 wt% nanosized TiC_p refined recrystallized grain from 41 μm to 13 μm, and the contribution on the increase in the yield strength can be described by the Hall-Petch equation: $\bar{\sigma}_{HP}=k/\sqrt{d}$ [29], where k is a constant and d is the average grain diameter. For Al alloy, k is found to be ~0.08 MPa $\sqrt{m}$ [30]. $\bar{\sigma}_{HP}$ is calculated to be ~12 MPa and ~22 MPa in the matrix 6061 Al alloy and 1.0–6061 Al, respectively. The increase contributed by the grain refinement is ~10 MPa.

The nanosized TiC_p in this paper are equiaxed and small enough so that the increase due to the Orowan stress (σ_{Orowan}) can be estimated by [31]:

$$\sigma_{\mathrm{Orowan}} = 0.81\frac{\mathrm{MAGb}}{2\pi\lambda}\ln\left(\frac{\pi d}{4b}\right) \quad (1)$$

where M is the Taylor factor (it was 3.06 for face-centred cubic metals), G is the shear modulus of the matrix (for pure aluminium at 298 K, $G \approx$

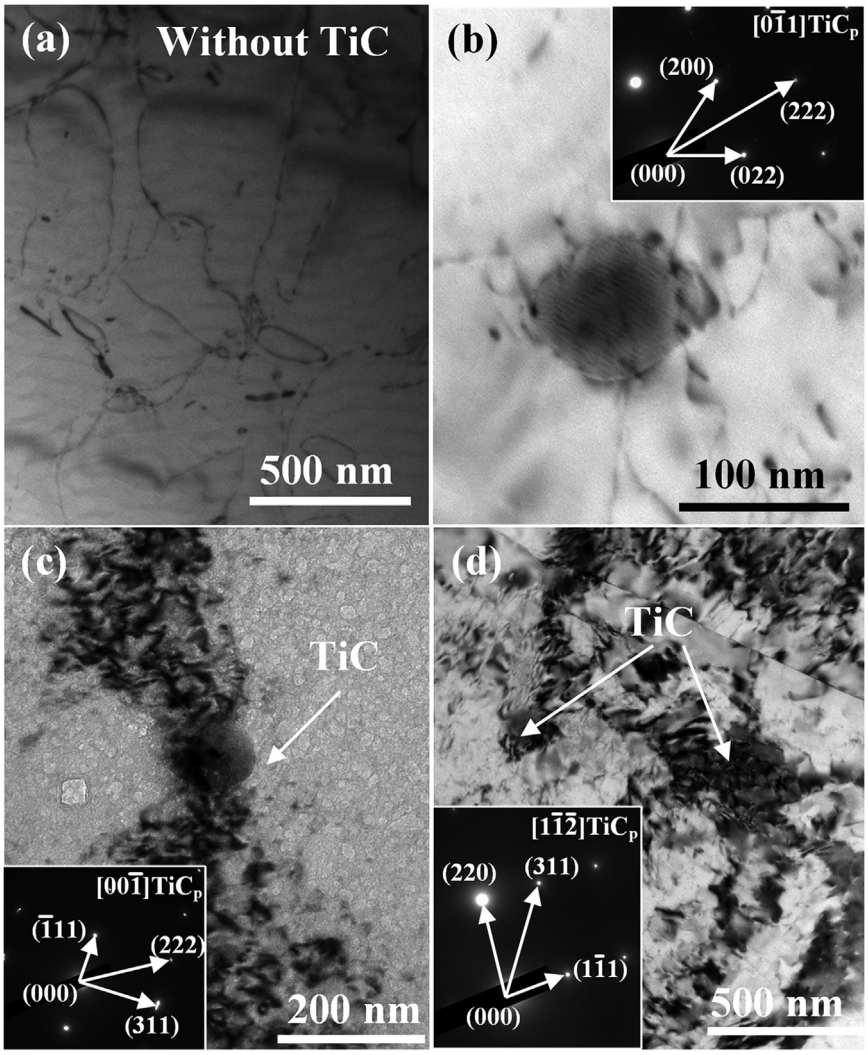

Fig. 7. TEM micrographs of the dislocations in SR samples: the dislocation in the 6061 Al alloy (a); nanosized TiC_p impede the movement of dislocations, forming dislocation tangles around the nanosized TiC_p (b)-(d).

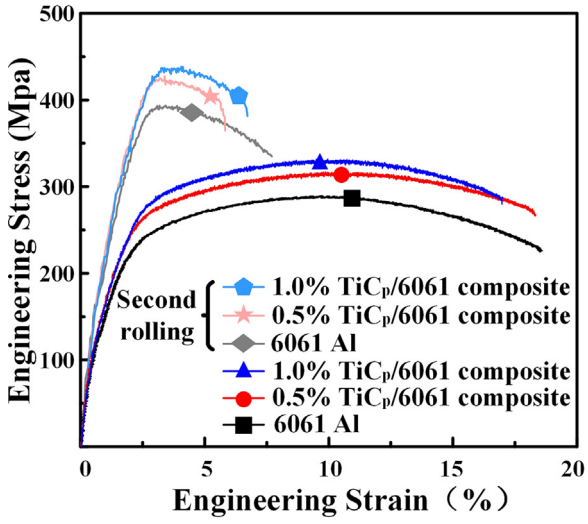

Fig. 8. Typical engineering stress-strain curves of the matrix 6061 Al alloy and the nanosized TiC_p/6061 composites with different fractions of the nanosized TiC_p.

Table 1
The ultimate tensile strength, yield strength and fracture strain of the matrix 6061 Al alloy and the nanosized TiC_p/6061 composites with different fractions of the nanosized TiC_p through different rolling processes.

	σ_b (MPa)	σ_s (MPa)	ε (%)
6061 Al (CR-T6)	288 ± 3	237 ± 3	18.6 ± 1.0
0.5–6061 (CR-T6)	315 ± 2	267 ± 4	18.4 ± 1.2
1.0–6061 (CR-T6)	330 ± 2	275 ± 3	17.9 ± 0.6
6061 Al (SR)	397 ± 1	374 ± 3	7.7 ± 0.5
0.5–6061 (SR)	427 ± 2	414 ± 3	5.8 ± 1.0
1.0–6061 (SR)	438 ± 2	426 ± 4	6.7 ± 1.1

25232 MPa [32]), b is the Burger's vector (b = 0.286 nm for Al). The constant A is estimated to be 1.2 [31]. λ is the interparticle spacing and d is the average particulate diameter. The calculation of λ can be described as the equation:

$$\lambda = 0.4d(\sqrt{\pi/fV}\text{-}2) \quad (2)$$

where f is the volume fraction of the TiC_p. For the simplicity of calculation, it is assumed that the nanoparticles distributed uniformly in the matrix. The calculated increase in 1.0–6061 Al is ~21.9 MPa. The actual distribution of the reinforcement is not randomly uniform, and some TiC_p were observed at grain boundaries (Fig. 5), reducing the

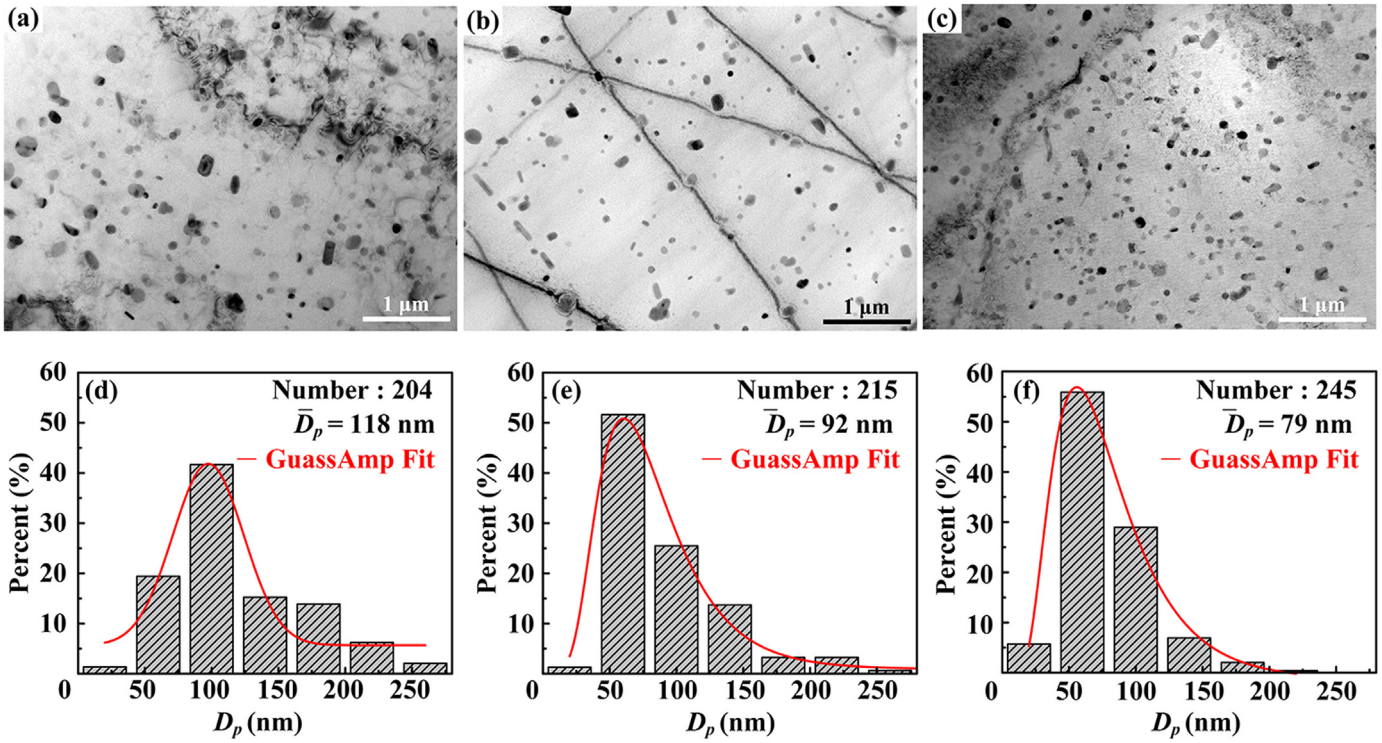

Fig. 9. TEM micrographs of the 6061 Al alloy and composites after T6 treatment: (a) the 6061 Al alloy, (b) the 0.5 wt% TiC_p/6061 composite and the (c) 1.0 wt% TiC_p/6061 composite; (d)-(f) the diameter distributions of the precipitates in (a)-(c), respectively.

effective amount of the nanosized TiC_p for Orowan strengthening.

Researchers reported that the introduction of the reinforcement particles can affect the precipitation of the composite significantly in comparison with the matrix alloys [33,34]. The rolling process induces high-density dislocations which contributes to the increased strength of the matrix 6061 Al alloy and the composites. The extra dislocations are retained around the nanoparticles, acting as the heterogeneous nucleation sites for precipitates, or the diffusion path for the solute atoms to improve the ageing kinetics of the composites during the T6 treatment. Fig. 9(a)-(c) shows the Mg_2Si precipitates in the matrix alloy, 0.5–6061 Al and 1.0–6061 Al, respectively. The distributions of the precipitates were reported in the form of histograms in Fig. 9(d)-(f). The red lines were the lognormal fit of the data, indicating the precipitates fitted a lognormal distribution. The mean size of precipitates were 118 nm, 92 nm and 79 nm for the matrix alloy, 0.5–6061 Al and 1.0–6061 Al, respectively. Clearly, the introduction of nanosized TiC_p resulted in a decrease in the precipitate diameter and an increase in the density of the precipitates. The precipitation strengthening was resulted from the restriction of precipitates to the bypassing dislocations. The strength increase caused by the precipitates strengthening can be calculated based on the modified Orowan equation [35]. Tian et al. [14] reported that the improvement contributed from the precipitates increased with the decrease in the diameters of precipitates according to these modified Orowan equation. It indicates that the smaller precipitates in the 1.0–6061 Al could play a more obvious effect to impede the dislocation movement, which is beneficial for improving the tensile strength.

As mentioned above, dislocations interact with each other and form the dislocation tangles in CR-T6 samples during the tensile process, which retards the dislocation movement. As a result, the dislocation walls were generated. The nanosized TiC_p could also act as a barrier to hinder the dislocation movement. Thus, the extra dislocation multiplication caused by the nanosized TiC_p contributes to the increase in the tensile strength. After the SR process, the sub-structures and high-density dislocations are formed as indicated in Fig. 7. On the one hand, the nanosized TiC_p could accelerate the formation of dislocations in the nanosized TiC_p/6061 composite resulting by the interaction between dislocations and TiC_p (Fig. 7(b)-(d)) [36]. On the other hand, with the Zener pinning effect, the particles can effectively impede the movement of dislocations. As a result, the dislocation strengthening contributes to the increase of the UTS and YS and results in a low elongation in the SR samples.

4. Conclusions

a. 1.0 wt% nanosized TiC_p refined the grain structure from 108 μm to 40.1 μm during the solidification process. The nanosized TiC_p retarded the recrystallization and grain growth during the T6 treatment, resulting in the refined recrystallization grains. The recrystallized grain size of the matrix alloy was 41 μm, and 13 μm for the 1.0–6061 Al.

b. The UTS and YS of the matrix 6061 Al alloy in CR-T6 state were 288 MPa and 237 MPa, respectively. The UTS and YS of the composites in CR-T6 state could reach 330 MPa and 275 MPa, respectively after adding 1.0 wt% nanosized TiC_p. Moreover, the ductility remained unchanged.

c. The UTS and YS of the matrix 6061 Al alloy were 397 MPa and 374 MPa, respectively after the SR process. The introduction of the nanosized TiC_p increased the tensile strength. They could reach 438 MPa and 426 MPa, respectively after adding 1.0 wt% nanosized TiC_p. However, the ductility was not improved.

d. The increase in the tensile strength of the CR-T6 samples at room temperature was attributed to the strengthening effect of the nanosized TiC_p, larger number of finer precipitates and the dislocation accumulation, collectively. These contributed to the enhanced tensile strengths without obviously reducing the ductility. The increased dislocation density in SR samples resulted in a slight reduction in ductility.

Acknowledgements

This work is supported by the National Natural Science Foundation of China (No.51571101 and No. 51601066), and the Science and Technology Development Program of Jilin Province, China (Grant Nos. 20160520116JH and 20170101215JC).

References

[1] Y.C. Lin, S.C. Luo, L.X. Yin, J. Huang, Microstructural evolution and high temperature flow behaviors of a homogenized Sr-modified Al-Si-Mg alloy, J. Alloy. Compd. 739 (2018) 590–599, https://doi.org/10.1016/j.jallcom.2017.12.278.
[2] K. Hamad, H.W. Yang, Y.G. Ko, Interpretation of annealing texture changes of severely deformed Al-Mg-Si alloy, J. Alloy. Compd. 687 (2016) 300–305, https://doi.org/10.1016/j.jallcom.2016.06.101.
[3] Y. Zhao, X. Ma, X. Zhao, H. Chen, X. Liu, Enhanced aging kinetic of Al3BC/6061 Al composites and its micro-mechanism, J. Alloy. Compd. 726 (2017) 1053–1061, https://doi.org/10.1016/j.jallcom.2017.08.053.
[4] V.K. Barnwal, R. Raghavan, A. Tewari, K. Narasimhan, S.K. Mishra, Effect of microstructure and texture on forming behaviour of AA-6061 aluminium alloy sheet, Mater. Sci. Eng. A 679 (2017) 56–65, https://doi.org/10.1016/j.msea.2016.10.027.
[5] A.J. Knowles, X. Jiang, M. Galano, F. Audebert, Microstructure and mechanical properties of 6061 Al alloy based composites with SiC nanoparticles, J. Alloy. Compd. 615 (2014) S401–S405, https://doi.org/10.1016/j.jallcom.2014.01.134.
[6] A. Mandal, R. Maiti, M. Chakraborty, B.S. Murty, Effect of TiB2 particles on aging response of Al-4Cu alloy, Mater. Sci. Eng. A 386 (2004) 296–300, https://doi.org/10.1016/j.msea.2004.07.026.
[7] S.Y. Qin, C.R. Chen, G.D. Zhang, W.L. Wang, Z.G. Wang, The effect of particle shape on ductility of SiCp reinforced 6061 Al matrix composites, Mater. Sci. Eng. A 272 (1999) 363–370, https://doi.org/10.1016/S0921-5093(99)00503-1.
[8] W.S. Tian, D.S. Zhou, F. Qiu, Q.C. Jiang, Superior tensile properties of in situ nano-sized TiCp/Al-Cu composites fabricated by reaction in melt method, Mater. Sci. Eng. A 658 (2016) 409–414, https://doi.org/10.1016/j.msea.2016.02.015.
[9] G.A. Bagheri, The effect of reinforcement percentages on properties of copper matrix composites reinforced with TiC particles, J. Alloy. Compd. 676 (2016) 120–126, https://doi.org/10.1016/j.jallcom.2016.03.085.
[10] H. Ghazanfari, C. Blais, H. Alamdari, M. Gariépy, R. Schulz, Mechanically activated combustion synthesis of Fe_3Al composite powders reinforced with sub-micrometer TiC particles, J. Alloy. Compd. 761 (2018) 71–79, https://doi.org/10.1016/j.jallcom.2018.05.145.
[11] K.B. Nie, X.J. Wang, X.S. Hu, L. Xu, K. Wu, M.Y. Zheng, Microstructure and mechanical properties of SiC nanoparticles reinforced magnesium matrix composites fabricated by ultrasonic vibration, Mater. Sci. Eng. A 528 (2011) 5278–5282, https://doi.org/10.1016/j.msea.2011.03.061.
[12] R. Casati, A. Fabrizi, G. Timelli, A. Tuissi, M. Vedani, Microstructural and mechanical properties of Al-based composites reinforced with in-situ and ex-situ Al_2O_3 nanoparticles, Adv. Eng. Mater. 18 (2016) 550–558, https://doi.org/10.1002/adem.201500297.
[13] X. Jiang, M. Galano, F. Audebert, Extrusion textures in Al, 6061 alloy and 6061/SiCp nanocomposites, Mater. Charact. 88 (2014) 111–118, https://doi.org/10.1016/j.matchar.2013.11.009.
[14] W.S. Tian, Q.L. Zhao, Q.Q. Zhang, F. Qiu, Q.C. Jiang, Enhanced strength and ductility at room and elevated temperatures of Al-Cu alloy matrix composites reinforced with bimodal-sized TiCp compared with monomodal–sized TiC p, Mater. Sci. Eng. A 724 (2018) 368–375, https://doi.org/10.1016/j.msea.2018.03.106.
[15] W.S. Tian, D.S. Zhou, F. Qiu, Q.C. Jiang, Superior tensile properties of in situ nano-sized TiCp/Al-Cu composites fabricated by reaction in melt method, Mater. Sci. Eng. A 658 (2016) 409–414, https://doi.org/10.1016/j.msea.2016.02.015.
[16] L.J. Zhang, F. Qiu, J.G. Wang, Q.C. Jiang, High strength and good ductility at elevated temperature of nano-SiCp/Al2014 composites fabricated by semi-solid stir casting combined with hot extrusion, Mater. Sci. Eng. A 626 (2015) 338–341, https://doi.org/10.1016/j.msea.2014.12.089.
[17] X.C. Tong, A.K. Ghosh, Fabrication of in situ TiC reinforced aluminum matrix composites, J. Mater. Sci. 36 (2001) 4059–4069, https://doi.org/10.1023/A:1017946927566.
[18] M. Karbalaei Akbari, H.R. Baharvandi, K. Shirvanimoghaddam, Tensile and fracture behavior of nano/micro TiB_2 particle reinforced casting A356 aluminum alloy composites, Mater. Des. 66 (2015) 150–161, https://doi.org/10.1016/j.matdes.2014.10.048.
[19] M.P. Reddy, R.A. Shakoor, G. Parande, V. Manakari, F. Ubaid, A.M.A. Mohamed, M. Gupta, Enhanced performance of nano-sized SiC reinforced Al metal matrix nanocomposites synthesized through microwave sintering and hot extrusion techniques, Prog. Nat. Sci. Mater. Int. 27 (2017) 606–614, https://doi.org/10.1016/j.pnsc.2017.08.015.
[20] Y. Zhao, X. Ma, H. Chen, X. Zhao, X. Liu, Preferred orientation and interfacial structure in extruded nano-Al_3BC/6061 Al, Mater. Des. 131 (2017) 23–31, https://doi.org/10.1016/j.matdes.2017.05.088.
[21] L. Wang, F. Qiu, Q.L. Zhao, H.Y. Wang, Q.C. Jiang, Simultaneously increasing the elevated-temperature tensile strength and plasticity of in situ nano-sized TiCx/Al-Cu-Mg composites, Mater. Charact. 125 (2017) 7–12, https://doi.org/10.1016/j.matchar.2017.01.013.
[22] J. Geng, T. Hong, Y. Shen, G. Liu, C. Xia, D. Chen, M. Wang, H. Wang, Microstructural stability of in-situ TiB_2/Al composite during solution treatment, Mater. Charact. 124 (2017) 50–57, https://doi.org/10.1016/j.matchar.2016.11.032.
[23] C.Y. Dan, Z. Chen, G. Ji, S.H. Zhong, Y. Wu, F. Brisset, H.W. Wang, V. Ji, Microstructure study of cold rolling nanosized in-situ TiB2particle reinforced Al composites, Mater. Des. 130 (2017) 357–365, https://doi.org/10.1016/j.matdes.2017.05.076.
[24] X. Yao, Z. Zhang, Y.F. Zheng, C. Kong, M.Z. Quadir, J.M. Liang, Y.H. Chen, P. Munroe, D.L. Zhang, Effects of SiC nanoparticle content on the microstructure and tensile mechanical properties of ultrafine grained AA6063-SiCnp nanocomposites fabricated by powder metallurgy, J. Mater. Sci. Technol. 33 (2017) 1023–1030, https://doi.org/10.1016/j.jmst.2016.09.022.
[25] T. Hong, Y. Shen, J. Geng, D. Chen, X. Li, C. Zhou, Effect of cryogenic pre-treatment on aging behavior of in-situ TiB2/Al-Cu-Mg composites, Mater. Charact. 119 (2016) 40–46, https://doi.org/10.1016/j.matchar.2016.07.012.
[26] J. Geng, G. Liu, F. Wang, T. Hong, C. Xia, M. Wang, D. Chen, N. Ma, H. Wang, Microstructural and mechanical anisotropy of extruded in-situ TiB_2/2024 composite plate, Mater. Sci. Eng. A 687 (2017) 131–140, https://doi.org/10.1016/j.msea.2017.01.069.
[27] W.S. Tian, Q.L. Zhao, Q.Q. Zhang, F. Qiu, Q.C. Jiang, Superior creep resistance of 0.3 wt% nano-sized TiCp/Al-Cu composite, Mater. Sci. Eng. A 700 (2017) 42–48, https://doi.org/10.1016/j.msea.2017.05.101.
[28] R.D. Doherty, D.A. Hughes, F.J. Humphreys, J.J. Jonas, D.J. Jensen, M.E. Kassner, W.E. King, T.R. McNelley, H.J. McQueen, A.D. Rollett, Current issues in recrystallization: a review, Mater. Sci. Eng. A 238 (1997) 219–274, https://doi.org/10.1016/S0921-5093(97)00424-3.
[29] A. Aversa, G. Marchese, M. Lorusso, F. Calignano, S. Biamino, E.P. Ambrosio, D. Manfredi, P. Fino, M. Lombardi, M. Pavese, Microstructural and mechanical characterization of aluminum matrix composites produced by laser powder bed fusion, Adv. Eng. Mater. 19 (2017) 1700180, https://doi.org/10.1002/adem.201700180.
[30] T. Shanmugasundaram, M. Heilmaier, B.S. Murty, V.S. Sarma, On the Hall-Petch relationship in a nanostructured Al-Cu alloy, Mater. Sci. Eng. A 527 (2010) 7821–7825, https://doi.org/10.1016/j.msea.2010.08.070.
[31] Q.L. Zhao, H. Zhang, X.X. Zhang, F. Qiu, Q.C. Jiang, Enhanced elevated-temperature mechanical properties of Al-Mn-Mg containing TiC nano-particles by pre-strain and concurrent precipitation, Mater. Sci. Eng. A 718 (2018) 305–310, https://doi.org/10.1016/j.msea.2018.01.123.
[32] A. Sanaty-Zadeh, Comparison between current models for the strength of particulate-reinforced metal matrix nanocomposites with emphasis on consideration of Hall-Petch effect, Mater. Sci. Eng. A 531 (2012) 112–118, https://doi.org/10.1016/j.msea.2011.10.043.
[33] A. Mandal, M. Chakraborty, B.S. Murty, Ageing behaviour of A356 alloy reinforced with in-situ formed TiB_2 particles, Mater. Sci. Eng. A 489 (2008) 220–226, https://doi.org/10.1016/j.msea.2008.01.042.
[34] R. Dong, W. Yang, Z. Yu, P. Wu, M. Hussain, L. Jiang, G. Wu, Aging behavior of 6061Al matrix composite reinforced with high content SiC nanowires, J. Alloy. Compd. 649 (2015) 1037–1042, https://doi.org/10.1016/j.jallcom.2015.07.233.
[35] W.S. Tian, Q.L. Zhao, R. Geng, F. Qiu, Q.C. Jiang, Improved creep resistance of Al-Cu alloy matrix composite reinforced with bimodal-sized TiCp, Mater. Sci. Eng. A 713 (2018) 190–194, https://doi.org/10.1016/j.msea.2017.12.071.
[36] Y.H. Zhao, J.F. Bingert, X.Z. Liao, B.Z. Cui, K. Han, A.V. Sergueeva, A.K. Mukherjee, R.Z. Valiev, T.G. Langdon, Y.T. Zhu, Simultaneously increasing the ductility and strength of ultra-fine-grained pure copper, Adv. Mater. 18 (2006) 2949–2953, https://doi.org/10.1002/adma.200601472.